Discovery of Two-Dimensional Electromagnetic Plasma Waves

A. Shuvaev,[1,*] V. M. Muravev,[2,*] P. A. Gusikhin,[2] J. Gospodarič,[1] A. Pimenov,[1] and I. V. Kukushkin[2]
[1]Institute of Solid State Physics, Vienna University of Technology, 1040 Vienna, Austria
[2]Institute of Solid State Physics, RAS, Chernogolovka 142432, Russia

(Received 7 November 2020; accepted 5 March 2021; published 31 March 2021)

We report the experimental discovery of "superluminal" electromagnetic 2D plasma waves in the electromagnetic response of a high-quality GaAs/AlGaAs two-dimensional electron system on a dielectric substrate. We measure the plasma wave spectrum on samples with different electron density. It is established that, at large two-dimensional densities, there is a strong hybridization between the plasma and the Fabry-Perot light modes. In the presence of a perpendicular magnetic field, the plasma resonance is shown to split into two modes, each corresponding to a particular sense of circular polarization. Experimental results are found to be in good agreement with the theory.

DOI: 10.1103/PhysRevLett.126.136801

Plasma waves in a two-dimensional electron system (2DES) were first predicted in 1967 [1], and then, ten years later, discovered experimentally in a sheet of electrons on the surface of liquid helium [2] as well as in a (100) silicon inversion layer [3,4]. These experiments, along with numerous subsequent studies [5–12] quantitatively confirmed the theoretical prediction of the 2D plasmon spectrum

$$\omega_p(q) = \sqrt{\frac{n_s e^2 q}{2m^*\varepsilon_0\varepsilon(q)}} \quad (q \gg \omega_p/c), \tag{1}$$

where q is the wave vector of the plasma wave lying in the plane of the 2DES, n_s and m^* are the density and effective mass of the electrons, and $\varepsilon(q)$ is the effective dielectric permittivity of the medium hosting the 2DES. Dielectric environment $\varepsilon(q)$ significantly affects the properties of 2D plasmons. For example, a uniform metallic gate situated close to the 2DES makes the dispersion of plasmons linear [13]. In turn, metal grating on top of the crystal may couple incident radiation to plasmons with large wave vectors. In this regime, nonlocal effects start to play the major role leading to the observation of Bernstein modes [14–16]. The 2D plasmons are longitudinal waves bound to the two-dimensional electron layer. In case of the 2DES layer placed in the vacuum, the localization of this wave $e^{-q_z|z|}$ is given by $q_z = \sqrt{q^2 - \omega_p^2/c^2}$. Therefore, this type of plasma wave has a "subluminal" nature $\omega_p < cq$, where c is the velocity of light.

Recently, it has been predicted that there is a second class of 2D plasma excitations—superluminal plasma waves [17]. As opposed to the electrostatic 2D plasmons [1–4], these are transverse electromagnetic waves propagating in a complex system including an infinite 2DES on a dielectric substrate. Interestingly, their spectrum $\omega_p(q) = \sqrt{\omega_p^2 + c^2q^2}$. Here, $\omega_p(q)$ is frequency at which electromagnetic radiation is resonantly transmitted through the substrate, and q is the wave vector in the 2DES plane. Note that the phase velocity v_φ of electromagnetic plasma waves is greater that the velocity of light $v_\varphi = \omega_p(q)/q > c$. The superluminal nature of these waves does not contradict physical laws, since their group velocity $v_g = d\omega_p(q)/dq = c^2/v_\varphi < c$.

In a case of a thin dielectric substrate $\omega_p \ll c/\sqrt{\varepsilon}d$, the superluminal plasma frequency is given by [18,19]

$$\omega_p \approx \omega_0 = \sqrt{\frac{n_s e^2}{m^*\varepsilon_0(\varepsilon - 1)d}}, \tag{2}$$

where d and ε denote the thickness and dielectric permittivity of the substrate.

In the present Letter, we report on the experimental discovery of superluminal plasma waves in the transmission spectrum of a 2DES on a dielectric substrate. In our experiments, the plasma resonance manifests itself as a maximum in the transmission of electromagnetic radiation through the sample. The radiation is incident perpendicular to the sample surface, therefore the in plane wave vector $q = 0$ and the resonant frequency $\omega = \omega_p$. It is established that there is a strong hybridization between the plasma and Fabry-Perot light modes $\omega_N = N\omega_d = N\pi c/(\sqrt{\varepsilon}d)$ $(N = 0, 1, 2\ldots)$. In particular, we have found that, at low electron density, the fundamental plasma resonance originates from $N = 0$ Fabry-Perot mode, whereas with increasing density, it tends to $\lambda/4$ resonance of the dielectric Fabry-Perot etalon. In the presence of a finite magnetic field, the plasma resonance is shown to split into two modes, with each one excited in a particular direction

of circular polarization. We demonstrate our experimental findings to be in good agreement with the recently developed theory [17].

In our study, we use the experimental setup depicted schematically in Fig. 1. A 1×1 cm^2 sample is mounted on a sample holder with a 10 mm pinhole at the location of the sample. The entire arrangement is oriented in the Faraday geometry inside an optical cryostat, with a split coil providing the magnetic field of up to ± 7 T applied perpendicular to the sample surface. The cryostat is equipped with 100 μm thick Mylar inner and outer windows, where the outer openings are covered with black polyethylene foil to block the visible light. The sample is illuminated with terahertz radiation incident parallel to the direction of the magnetic field. Continuous monochromatic radiation is generated by backward-wave oscillators (BWOs) operating in the submillimeter frequency range of 20–600 GHz. The signal transmitted through the sample is detected by a He-cooled bolometer. The measurements are taken either by sweeping the frequency at a fixed magnetic field or by sweeping the magnetic field at several fixed frequencies. The samples used to produce the presented data are cleaved from three different GaAs wafers, with each specimen polished down to the thickness of around 0.2 mm. Two wafers contain a single 20 nm wide $Al_{0.24}Ga_{0.76}As/GaAs/Al_{0.24}Ga_{0.76}As$ quantum well grown by molecular beam epitaxy 200 nm below the crystal surface. The two wafers have 2D electron densities of $n_{s1} = 1.4 \times 10^{11}$ and $n_{s2} = 1.4 \times 10^{12}$ cm^{-2}, with respective electron mobilities derived from high-frequency data, $\mu = 0.7 \times 10^6$ and 80×10^3 cm^2/V s. The third wafer contains five 20 nm wide quantum wells spaced 60 nm apart, with total electron density $n_{s3} = 6.4 \times 10^{12}$ cm^{-2} and electron mobility $\mu = 60 \times 10^3$ cm^2/V s. All measurements are conducted at the base sample temperature of $T = 5$ K.

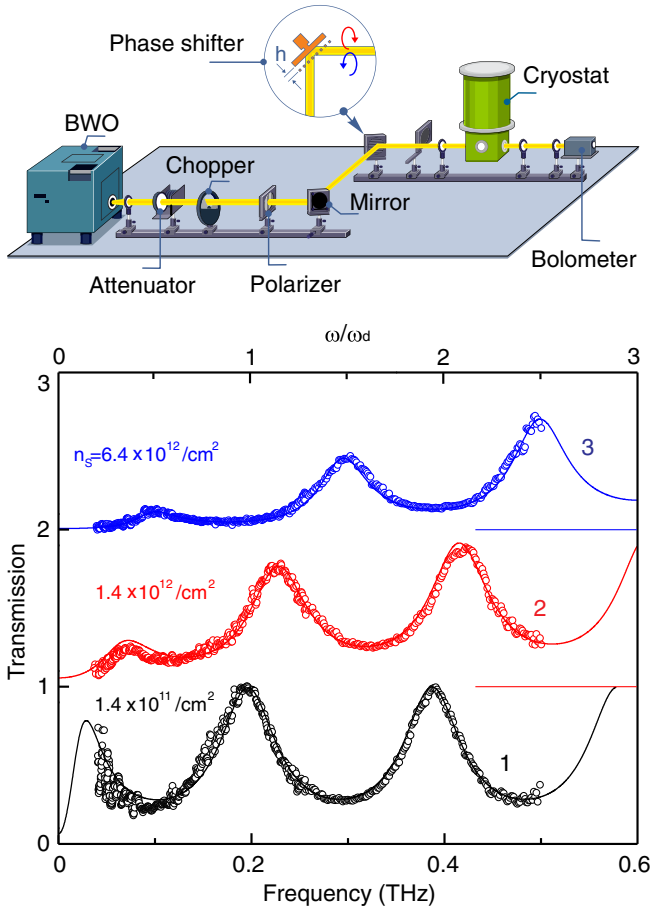

FIG. 1. Top: diagram of the experimental setup. Bottom: transmission data for three samples with different electron densities n_s. The curves are offset vertically for clarity purposes. Solid lines correspond to the theoretical prediction based on the Drude model of the dynamic conductivity in the quasiclassical approximation. The upper horizontal axis shows the normalized frequency ω/ω_d, where $\omega_d = \pi c/\sqrt{\epsilon} d$ is the frequency of the first Fabry-Perot mode for the GaAs substrate of thickness $d = 0.21$ mm.

Figure 1 shows transmission spectra obtained for three samples with different electron densities and slightly varied GaAs substrate thickness of $d_1 = 212$ μm (black dots), $d_2 = 200$ μm (red dots), and $d_3 = 191$ μm (blue dots). The measurements are conducted for the linearly polarized incident radiation, at zero external magnetic field $B = 0$ T. As a result, we observe that the presence of 2D plasma leads to a blueshift in $N = 1$ and $N = 2$ Fabry-Perot modes from their unperturbed position of $\omega_N = N\pi c/(\sqrt{\epsilon} d)$, given $\epsilon_{\mathrm{GaAs}} = 12.8$. The most striking discovery, however, is an additional resonance emerging in the low-frequency part of the spectra. Originating from the $N = 0$ Fabry-Perot mode, the transmission resonance undergoes a significant change in frequency with increasing electron density n_s, indicating the plasma nature of the phenomenon. We find the experimental data to be accurately described by the analytical model based on Drude dynamic conductivity in the quasiclassical approximation, plotted in solid lines in Fig. 1. For more details on the theoretical model, we refer the reader to the Supplemental Material [20]. Regarding the results for the small-density sample, we note that the resonance frequency $f_p = 24.8$ GHz is obtained by the extrapolation of the data using the theoretical prediction, followed by B-sweep measurements at frequencies $f < 50$ GHz.

Figure 2 displays the $N = 0$ resonance frequency as a function of n_s. Here, we include an extra data point corresponding to the electron density $n_s = 2.4 \times 10^{11}$ cm^{-2}, which was achieved by a short illumination of the sample with original density of 1.4×10^{11} cm^{-2} by a white light-emitting diode. It is evident that, in the limit of low electron density, the experimental data are well described by the theoretical prediction of the superluminal plasma frequency from Eq. (2), plotted in the dashed blue line in Fig. 2. Indeed, since the electromagnetic radiation is incident perpendicular

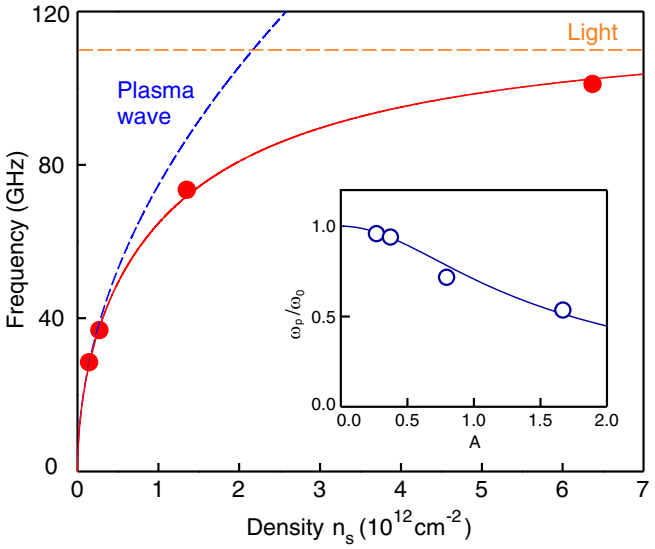

FIG. 2. Resonant frequency dependence on the electron density, n_s. The solid curve is calculated from Eq. (3). Dashed lines represent the non-retarded plasma frequency from Eq. (2), and the Fabry-Perot photon mode $\omega = \omega_d/2$. Inset shows the normalized plasma frequency ω_p/ω_0 versus the retardation parameter A.

to the sample surface, we excite an electromagnetic plasma wave with the in plane wave vector $q = 0$. On the other hand, when the electron density is increased, we observe that the resonance frequency tends to $\omega_d/2$—the fundamental frequency of the dielectric Fabry-Perot etalon. This result indicates the hybridization of the electromagnetic plasma wave ω_p and the Fabry-Perot light mode at $\omega = \omega_d/2$. The hybridization can be expressed elegantly by introducing a dimensionless retardation parameter $A = 2\omega_0/\omega_d$ defined as the ratio of the electrostatic plasma frequency from Eq. (2) to the frequency of light trapped in the substrate. Hence, given the introduced retardation parameter, we can express the normalized plasma frequency as follows [17]:

$$\frac{\omega_p}{\omega_0} = \frac{1}{\sqrt{1+A^2}}, \qquad \omega_0 = \sqrt{\frac{n_s e^2}{m^* \varepsilon_0 (\varepsilon - 1) d}}. \tag{3}$$

As shown in Fig. 2, the experimental data closely follow the solid curve calculated from Eq. (3) for the GaAs substrate thickness $d = 0.19$ mm. Furthermore, it should be noted that the expression similar to Eq. (3) is also valid for the TM plasmon-polariton excitations propagating along the 2DES [21–28]. However, considering the longitudinal plasmon polaritons, the 2D plasma wave couples to the light propagating along the plane of the 2DES rather than perpendicular to it, as in the case of the present investigation.

One of the most outstanding properties of the electromagnetic plasma waves is their strong coupling with cyclotron motion in the presence of the magnetic field. In Fig. 3, we plot the resonant transmission frequency

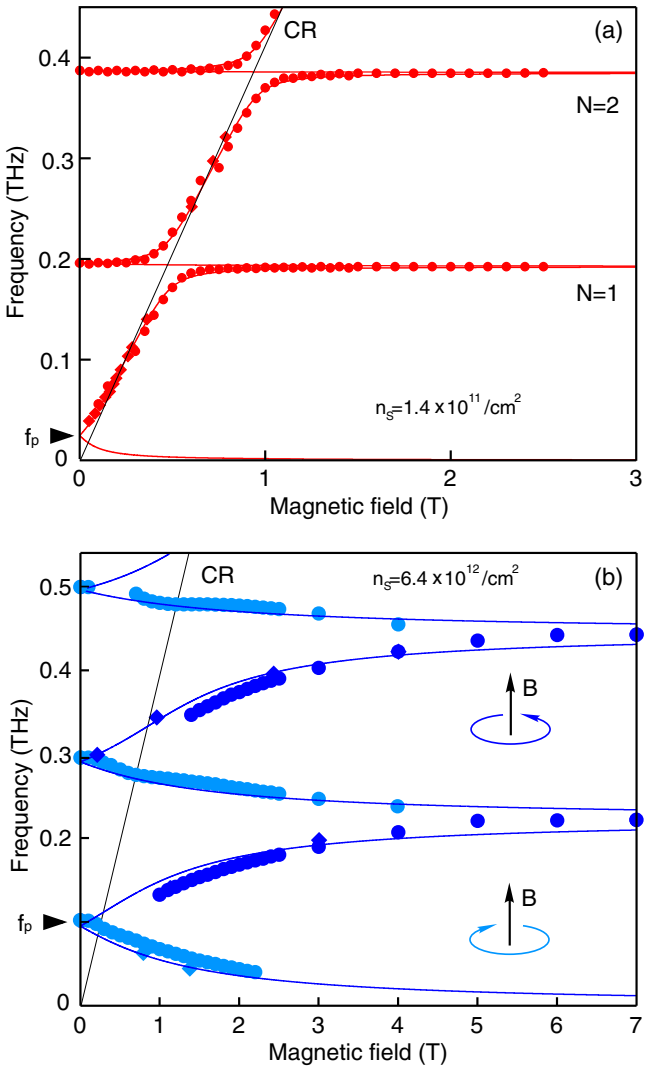

FIG. 3. Dependence of the resonant transmission frequency on the applied magnetic field. Plots (a) and (b) show experimental data obtained for the samples with 2D electron densities $n_{s1} = 1.4 \times 10^{11}$ and $n_{s3} = 6.4 \times 10^{12}$ cm^{-2}, accordingly. Circles correspond to frequency-sweep measurements taken with linearly polarized incident radiation. Diamonds denote the B-sweep data for the excitation radiation with a fixed sense of circular polarization.

as a function of the applied magnetic field, directed perpendicular to the sample surface. Experimental data in Figs. 3(a) and 3(b) correspond to the samples with electron densities $n_{s1} = 1.4 \times 10^{11}$ and $n_{s3} = 6.4 \times 10^{12}$ cm^{-2}, respectively. Magnetodispersion for the sample with $n_{s2} = 1.4 \times 10^{12}$ cm^{-2} is included in the Supplemental Material [20]. For each sample, we conducted two sets of measurements. For the first dataset (circles in Fig. 3), we swept the frequency of the incident linearly polarized radiation at a fixed magnetic field [see, for example, Fig. 4(a)]. The second dataset (diamonds in Fig. 3) was taken by sweeping the magnetic field at a constant radiation frequency [see, for example,

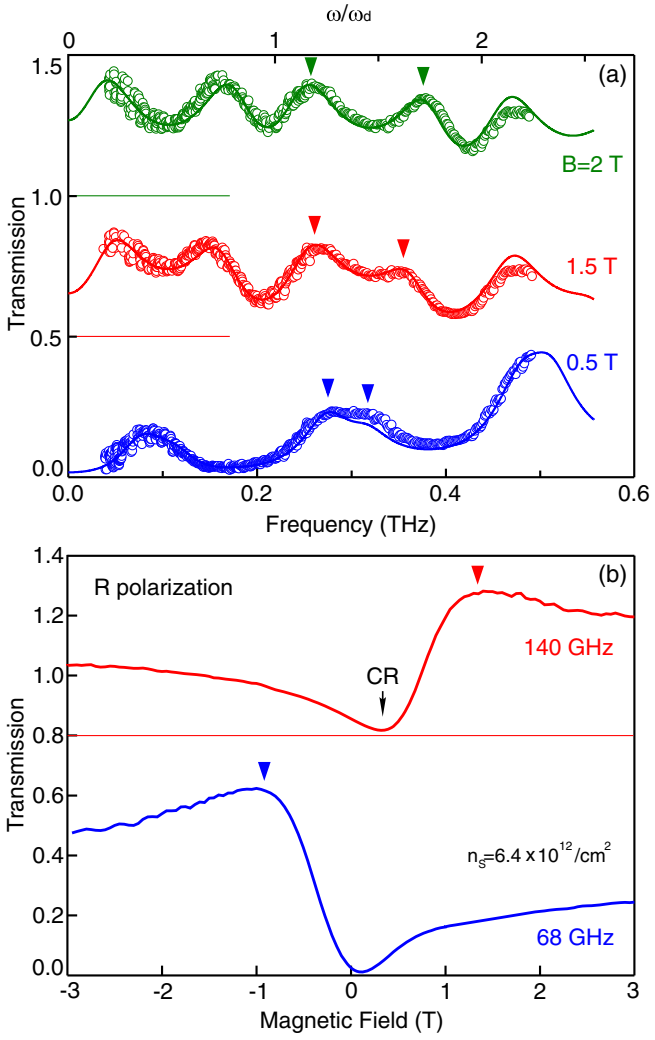

FIG. 4. (a) Transmission spectra at $B = 0.5$, 1.5, and 2 T for the sample with electron density $n_{s3} = 6.4 \times 10^{12}$ cm^{-2} and substrate thickness of $d_3 = 191$ μm. During the experiment, we used a linear polarization of incident electromagnetic radiation. Solid lines correspond to the theoretical prediction based on the Drude model. (b) B-sweep measurements for 68 and 140 GHz right-hand circular polarized radiation obtained for the same sample. The curves are offset for the clarity. The zero-transmission level for each curve is marked by a line.

Fig. 4(b)]. The second measurement scheme has two advantages. First, it enables registering the magnetodispersion of plasma excitation at frequencies below 50 GHz. Thus, we measured the plasma frequency of $f_p = (24.8 \pm 0.5)$ GHz for the sample with electron density of $n_{s1} = 1.4 \times 10^{11}$ cm^{-2} [arrow in Fig. 3(a)]. Second, the fixed frequency setup allows for controlling the sense of circular polarization.

Data in Fig. 3(a) display that transmission resonance corresponding to the excitation of the 2D electromagnetic plasma wave first occurs at $f_p = 24.8$ GHz (at $B = 0$ T) and then hybridizes rapidly with the cyclotron resonance (CR) $\omega_c = eB/m^*$ ($m^* = 0.067m_0$). Increasing the magnetic field further, we observe a series of anticrossings, typical of ultrastrong coupling between the cyclotron resonance and Fabry-Perot modes of the substrate [29–32]. Interestingly, the Rabi frequency of the observed coupling is exactly equal to the plasma frequency $\Omega_R = \omega_p$. Comparing the measurement results against the theoretical prediction of the magnetodispersion [17] (solid curves in Fig. 3), we see that experimental data are described very accurately by the theory.

What we find most intriguing, however, is the mode splitting, observed for the samples with large retardation $n_{s2} = 1.4 \times 10^{12}$ cm^{-2}, as discussed in Supplemental Material [20], and $n_{s3} = 6.4 \times 10^{12}$ cm^{-2}, as shown in Fig. 3(b). Considering the behavior of the fundamental ($N = 0$) plasma resonance, raising the external magnetic field leads to the split in the transmission resonance—the high-frequency mode moving past the CR, approaching the Fabry-Perot frequency ω_d [dark blue circles in Fig. 3(b)], and the low-frequency mode tending toward zero at an ever-decreasing rate [light blue circles in Fig. 3(b)]. Example transmission spectra measured for the sample with electron density $n_{s3} = 6.4 \times 10^{12}$ cm^{-2} are shown in Fig. 4(a). Importantly, circular polarization measurements reveal that the high-frequency mode is excited only by the R-polarized radiation when the electron cyclotron motion and radiation circulation directions coincide. In contrast, the low-frequency transmission peak occurs exclusively in the case of the L circular polarization. This result is counterintuitive since it is unexpected to see any response in a passive L polarization.

Thus far, in our analysis, we discussed only the transmission maxima, marked by the arrows in Fig. 4(b). As for the magnetodispersion of the transmission minima, it is found to follow closely the single-particle CR line $\omega_c = eB/m^*$. It can be shown that the 2DES absorption maxima also follow the single-particle CR in a zigzag way, as shown in the Supplemental Material [20]. Obtained experimental results explain the physical origin of the cyclotron resonance fine structure revealed recently in 2DESs [33]. The current work makes it evident that the single-particle CR observed in this Letter has a superluminal electromagnetic nature.

To summarize, we have experimentally discovered electromagnetic waves propagating in a complex system of 2D plasma on a dielectric substrate—the arrangement commonly used in semiconductor devices. We show that the spectrum of these electromagnetic waves has several unique features. First, it is superluminal, which is characteristic of the propagating modes. Second, the electromagnetic plasma waves exhibit strong hybridization with Fabry-Perot light modes. Finally, we demonstrate that, in the presence of a finite magnetic field, electromagnetic 2D plasma resonance splits into two modes, with each one excited in a particular direction of the circular polarization.

We thank V. A. Volkov and A. A. Zabolotnykh for the stimulating discussions. The authors gratefully acknowledge the financial support from the Russian Science Foundation (Grant No. 19-72-30003) and Austrian Science Fund (I3456-N27).

[*] A. S. and V. M. M. contributed equally to this work.

[1] F. Stern, Phys. Rev. Lett. **18**, 546 (1967).
[2] C. C. Grimes and G. Adams, Phys. Rev. Lett. **36**, 145 (1976).
[3] S. J. Allen, Jr., D. C. Tsui, and R. A. Logan, Phys. Rev. Lett. **38**, 980 (1977).
[4] T. N. Theis, J. P. Kotthaus, and P. J. Stiles, Solid State Commun. **24**, 273 (1977).
[5] U. Mackens, D. Heitmann, L. Prager, J. P. Kotthaus, and W. Beinvogl, Phys. Rev. Lett. **53**, 1485 (1984).
[6] D. C. Glattli, E. Y. Andrei, G. Deville, J. Poitrenaud, and F. I. B. Williams, Phys. Rev. Lett. **54**, 1710 (1985).
[7] W. F. Andress, H. Yoon, K. Y. M. Yeung, L. Qin, K. West, L. Pfeiffer, and D. Ham, Nano Lett. **12**, 2272 (2012).
[8] J. Chen, M. Badioli, P. Alonso-Gonzalez, S. Thongrattanasiri, F. Huth, J. Osmond, M. Spasenovic, A. Centeno, A. Pesquera, P. Godignon, A. Zurutuza Elorza, N. Camara, F. Abajo, R. Hillenbrand, and Frank H. L. Koppens, Nature (London) **487**, 77 (2012).
[9] Z. Fei, A. S. Rodin, G. O. Andreev, W. Bao, A. S. McLeod, M. Wagner, L. M. Zhang, Z. Zhao, M. Thiemens, G. Dominguez, M. M. Fogler, A. H. Castro Neto, C. N. Lau, F. Keilmann, and D. N. Basov, Nature (London) **487**, 82 (2012).
[10] G. C. Dyer, G. R. Aizin, S. J. Allen, A. D. Grine, D. Bethke, J. L. Reno, and E. A. Shaner, Nat. Photonics **7**, 925 (2013).
[11] Q. Shi, M. A. Zudov, L. N. Pfeiffer, K. W. West, J. D. Watson, and M. J. Manfra, Phys. Rev. B **93**, 165438 (2016).
[12] D. A. Bandurin, D. Svintsov, I. Gayduchenko, S. G. Xu, A. Principi, M. Moskotin, I. Tretyakov, D. Yagodkin, S. Zhukov, T. Taniguchi, K. Watanabe, I. V. Grigorieva, M. Polini, G. N. Goltsman, A. K. Geim, and G. Fedorov, Nat. Commun. **9**, 5392 (2018).
[13] A. V. Chaplik, Zh. Eksp. Teor. Fiz. **62**, 746 (1972) [Sov. Phys. JETP **35**, 395 (1972)].
[14] K. W. Chiu and J. J. Quinn, Phys. Rev. B **9**, 4724 (1974).
[15] E. Batke, D. Heitmann, J. P. Kotthaus, and K. Ploog, Phys. Rev. B **54**, 2367 (1985).
[16] E. Batke, D. Heitmann, and C. W. Tu, Phys. Rev. B **34**, 6951 (1986).
[17] P. A. Gusikhin, V. M. Muravev, and I. V. Kukushkin, Phys. Rev. B **102**, 121404(R) (2020).
[18] Yu. A. Kosevich, JETP Lett. **53**, 150 (1991).
[19] V. A. Volkov and V. N. Pavlov, JETP Lett. **99**, 93 (2014).
[20] See Supplemental Material at http://link.aps.org/supplemental/10.1103/PhysRevLett.126.136801 for detailed information on a theoretical model of the transmittance, additional experimental data, and analysis of the cyclotron frequency renormalization by retardation effects.
[21] V. I. Fal'ko and D. E. Khmel'nitskii, Zh. Eksp. Teor. Fiz. **95**, 1988 (1989) [Sov. Phys. JETP **68**, 1150 (1989)].
[22] A. O. Govorov and A. V. Chaplik, Sov. Phys. JETP **68**, 1143 (1989).
[23] I. V. Kukushkin, J. H. Smet, S. A. Mikhailov, D. V. Kulakovskii, K. von Klitzing, and W. Wegscheider, Phys. Rev. Lett. **90**, 156801 (2003).
[24] S. A. Mikhailov and N. A. Savostianova, Phys. Rev. B **71**, 035320 (2005).
[25] A. V. Chaplik, Pis'ma Zh. Eksp. Teor. Fiz. **101**, 602 (2015) [JETP Lett. **101**, 545 (2015)].
[26] T. Low, Pai-Yen Chen, and D. N. Basov, Phys. Rev. B **98**, 041403(R) (2018).
[27] D. O. Oriekhov and L. S. Levitov, Phys. Rev. B **101**, 245136 (2020).
[28] I. V. Andreev, V. M. Muravev, N. D. Semenov, and I. V. Kukushkin, Phys. Rev. B **103**, 115420 (2021).
[29] V. M. Muravev, I. V. Andreev, I. V. Kukushkin, S. Schmult, and W. Dietsche, Phys. Rev. B **83**, 075309 (2011).
[30] G. Scalari, C. Maissen, D. Turcinkova, D. Hagenmüller, S. De Liberato, C. Ciuti, C. Reichl, D. Schuh, W. Wegscheider, M. Beck, and J. Faist, Science **335**, 1323 (2012).
[31] Q. Zhang, M. Lou, X. Li, J. L. Reno, W. Pan, J. D. Watson, M. J. Manfra, and J. Kono, Nat. Phys. **12**, 1005 (2016).
[32] X. Li, M. Bamba, Q. Zhang, S. Fallahi, G. C. Gardner, W. Gao, M. Lou, K. Yoshioka, M. J. Manfra, and J. Kono, Nat. Photonics **12**, 324 (2018).
[33] V. M. Muravev, I. V. Andreev, S. I. Gubarev, V. N. Belyanin, and I. V. Kukushkin, Phys. Rev. B **93**, 041110(R) (2016).